Scripta Materialia 115 (2016) 133–136

Contents lists available at ScienceDirect

Scripta Materialia

journal homepage: www.elsevier.com/locate/scriptamat

Regular Article

High temperature shape memory behavior of $Ni_{50.3}Ti_{25}Hf_{24.7}$ single crystals

L. Patriarca [a], Y. Wu [a], Huseyin Sehitoglu [a,*], Y.I. Chumlyakov [b]

[a] Department of Mechanical Science and Engineering, University of Illinois at Urbana-Champaign, 1206 W. Green St., Urbana, IL 61801, USA
[b] Siberian Physical-Technical Institute of Tomsk State University, Tomsk 634050, Russia

ARTICLE INFO

Article history:
Received 11 December 2015
Received in revised form 9 January 2016
Accepted 9 January 2016
Available online 25 January 2016

Keywords:
Shape memory alloy
Single crystal
Transformation strain
X-ray diffraction
Digital image correlation

ABSTRACT

In this work we present the high temperature functional behavior of the new $Ni_{50.3}Ti_{25}Hf_{24.7}$ shape memory alloy (SMA). Very high transformation strains were measured during isobaric experiments at temperatures up to Af = 420 °C. For the $[111]_{B2}$ orientation in tension, we measured with digital image correlation (DIC) averaged transformation strain of 5.15%, while in small domains 7.74%. For the $[011]_{B2}$ orientation in compression, we measured averaged transformation strain of 4.6%, locally 5.3%. The remarkable results in terms of actuation strains at T > 400 °C define the $Ni_{50.3}Ti_{25}Hf_{24.7}$ alloy as one of the most promising shape SMA for high temperature applications.

1. Introduction

In the last years many efforts have been made to increment the transformation temperatures (TTs) of the NiTi system without compromising the functionality of the alloy. Ternary additions to the binary NiTi system have shown to enhance the operational temperatures [1]. In particular, substituting Hf for Ti represents one of the most effective and cost-sustainable solution. The transformation temperatures can reach values as high as 400 °C for Hf additions up to 30 at.% [2]. The beneficial effect of Hf additions on the transformation temperatures is counterbalanced by some drawbacks on the mechanical properties of NiTiHf alloys. In particular, NiTiHf polycrystals show low ductility and low transformation strains which limit their functionality. One possibility to circumvent these limitations is to study the single crystal behavior and properly select the crystal orientation that maximizes both the transformation strains and the slip resistance of the austenitic phase. In this work, we present for the first time the experimental results on the new $Ni_{50.3}Ti_{25}Hf_{24.7}$ alloy along the $[111]_{B2}$ orientation in tension and along the $[011]_{B2}$ orientation in compression. Isobaric experiments were conducted to establish the transformation strains. Remarkably, we found local transformation strains in tension up to 7.74% alongside the austenite finish temperature of Af = 422 °C. The results of the present study are summarized in Fig. 1 with conventional and high-temperatures shape memory alloys (SMAs). As shown in the schematic, the NiTiHf25 alloy represents, so far, the SMA with the largest transformation strain at operational temperatures T > 400 °C.

Depending on the chemistry, aging treatment and orientation, the transformation strain of NiTiHf alloys can be tailored based on the desired operational temperature and work output. Recently, NiTiHf alloys have been studied for Hf additions up to 20% [3–10]. It has been shown that high transformation strains (4%) can be reached at temperatures T < 200 °C for the $[011]_{B2}$ and $[111]_{B2}$ orientations of the $N_{i50.3}T_{i29.7}Hf_{20}$ composition [3]. For the same alloy, at higher temperatures (T < 250 °C), the $[340]_{B2}$ orientation displays transformation strains of 3.34% [4]. In our previous work, we show that with Hf addition up to 25%, locally, the polycrystalline $Ni_{50.6}Ti_{24.4}Hf_{25}$ can reach transformation strains up to 4.11% at temperatures higher than 250 °C [11]. This result promoted further research efforts on the $NiTiHf_{25}$ alloy as, potentially, these local strain measurements indicated that some orientations provide high transformation strains. We then grown single crystals of the new $Ni_{50.3}Ti_{25}Hf_{24.7}$ alloy after adjusting the Ni content (50.3 versus 50.6 at.%) in order to further increase the transformation temperatures. In order to maximize the transformation strains, we cut compression specimens along the $[011]_{B2}$ orientation and tensile specimens along the $[111]_{B2}$ orientation.

Isobaric experiments were conducted using advanced digital image correlation (DIC) strain measurements. As already shown in our previous works on other two NiTiHf compositions [11,12], DIC enables to capture the evolution of the local deformations. These strain measurements revealed the heterogeneity of the austenite–martensite phase transformation in the polycrystal case where the strain heterogeneity is mainly dictated by the grain orientation. In this work, we still used DIC to track local deformations during isobaric and isothermal experiments on the $Ni_{50.3}Ti_{25}Hf_{24.7}$ $[011]_{B2}$ single crystal. We defined the bulk strain as the averaged strain over the entire DIC region (3.8 mm × 2.6 mm), and the local strain as the strain calculated in

* Corresponding author.
E-mail address: huseyin@illinois.edu (H. Sehitoglu).

http://dx.doi.org/10.1016/j.scriptamat.2016.01.015
1359-6462/

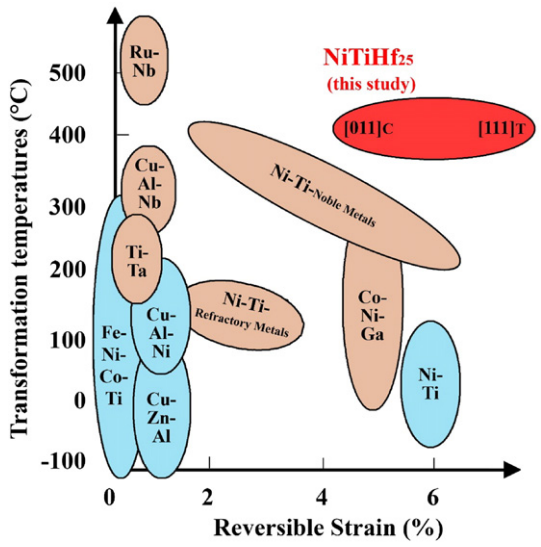

Fig. 1. The $NiTiHf_{25}$ alloy proposed in the present work compared with conventional (light blue) and high-temperature (light brown) shape memory alloys (the schematic was taken from [13]). At temperatures higher than 400 °C, the new $NiTiHf_{25}$ alloy shows the largest transformation strains.

small regions (1 mm × 0.6 mm). On a single crystal, the local strain measurements point to the maximum transformation strain measured over the sample avoiding to account for non-transforming regions.

In the following, we present the microstructural characterization of the B2 austenitic phase of the $Ni_{50.3}Ti_{25}Hf_{24.7}$ single crystal at high temperatures (from 500 °C) using X-ray diffraction. The results were also used to calculate the lattice constant for the B2 austenitic phase. Successively, the experimental transformation strains were determined from isobaric experiments.

2. Experiments

The initial $Ni_{50.3}Ti_{25}Hf_{24.7}$ single crystal ingot was grown by the Bridgman technique in He atmosphere. In the as grown conditions we initially measured the transformation temperatures using differential scanning calorimetry (DSC) by means of a Perkin Elmer Pyris 1 differential scanning calorimeter. We measured the austenite start temperature As = 251 °C, the austenite finish temperature Af = 422 °C, the martensite start temperature Ms. = 340 °C, and the martensite finish temperature Mf = 214 °C. The orientation of the single crystal was obtained at T = 500 °C in the fully austenitic phase (Fig. 2a). High temperature X-ray diffraction was performed on a Philips Xpert 2 diffractometer using Cu Kα radiation. The voltage was set to 45 kV, while the current was set to 40 MA. The inverse pole figures reported in Fig. 2a illustrate the crystal orientations in the x–y–z reference frame of the sample cut from the single crystal rod. Along the z direction, which is parallel to the load direction of the compression specimens (4 mm × 4 mm × 9 mm), the crystal is oriented parallel to the $[011]_{B2}$ direction. The y axis is parallel to the $[111]_{B2}$ orientation, and it defines the load direction for the tensile specimens (dog-bone shape with 1.5 mm × 3 mm gauge section). X-ray diffraction was also used to analyze the diffraction peaks in the austenitic phase (Fig. 2b). The peaks corresponding to the reflections of the $(011)_{B2}$ and $(022)_{B2}$ planes are indicated at 500 °C. The lattice parameter for the cubic B2 austenite is calculated as $a_0 = 3.075$ Å. During cooling, the diffraction pattern was captured every 50 °C in order to characterize the phase transformation. At room temperature, the $(011)_{B2}$ peak indicates that some residual austenitic phase is still present at room temperature.

The compression and tension specimens were sectioned by electrical discharge machining. Prior to loading, the specimens were manually

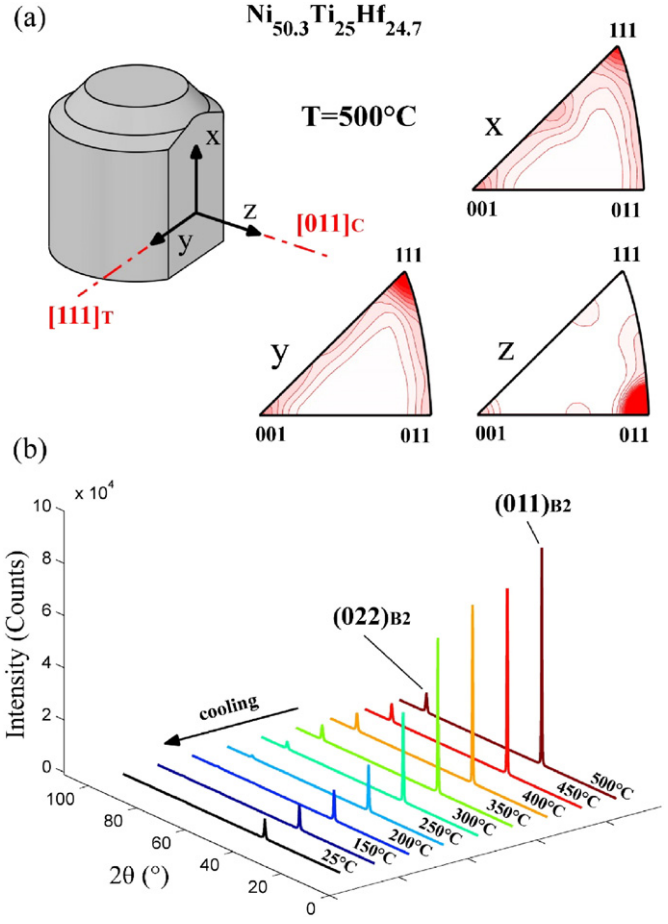

Fig. 2. Single crystal orientation and microstructural characterization of the austenitic phase at 500 °C. (a) The inverse pole figures obtained at 500 °C representing the crystal orientations of the sliced plane along the x, y and z directions. The compression specimens were cut with the loading direction parallel to the $[011]_{B2}$ orientation (z axis), while the loading direction of the tension specimens was parallel to the $[111]_{B2}$ orientation (y axis). (b) The X-ray diffraction pattern showing the peaks originated from the reflection of the $(011)_{B2}$ and $(022)_{B2}$ planes during cooling from 500 °C; the calculated lattice parameter of the cubic B2 austenite is $a_0 = 3.075$ Å at 500 °C.

polished with grid paper up to P1800. A fine speckle pattern was deposited on one side of the specimen using an Iwata Micron B airbrush and a black paint for high temperature applications. The speckle pattern enabled to capture images for DIC strain measurements with a resolution of 3 μm/px. The isobaric experiments were carried out by means of a MTS load frame. The temperature was measured with a Raytek infrared temperature camera. Strains were determined using in-situ DIC technique. During the isobaric experiments the reference image was captured at the initial temperature of the thermal cycle (maximum temperature) and at zero load. A second image was captured after the application of the isobaric stress at the same initial temperature. Successively, the images for DIC were manually captured during the cooling–heating cycles every 5 °C. The DIC strain fields reported in the following always refer to the axial component of the strain tensor parallel to the load direction.

3. Results

Fig. 3a shows the isobaric experiment conducted under the constant tensile stress of 300 MPa. We defined the bulk strain as the averaged strain over the DIC region of the specimen (3.8 mm × 2.6 mm), and the local strain as the averaged strain over a sub-region of the entire DIC area where the maximum strains are measured (1 mm × 0.4 mm). By using the local strain measurements, we provide the maximum transformation strain corresponding to the region where the austenite–

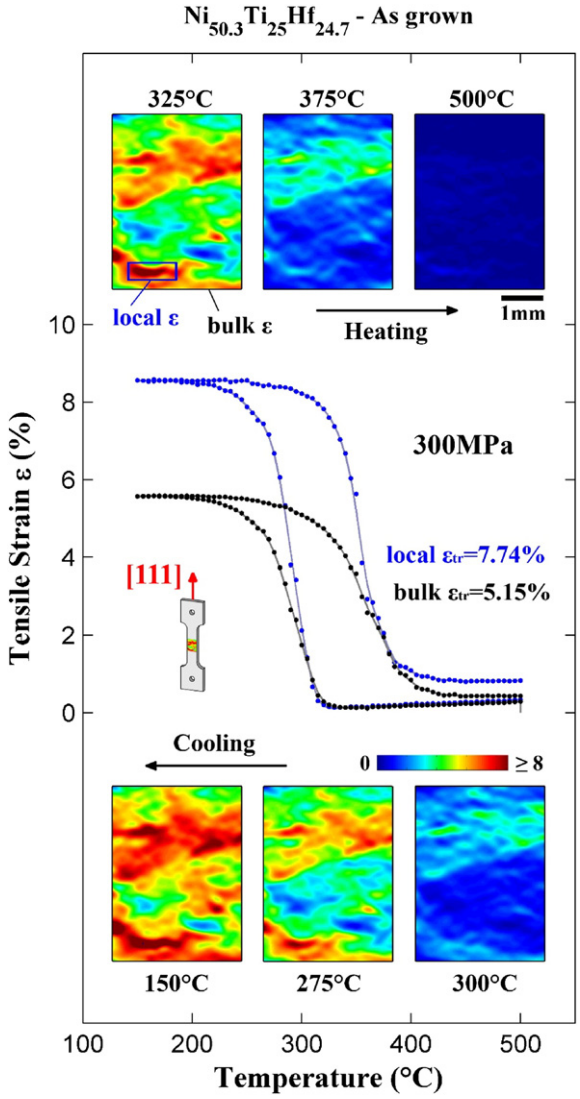

Fig. 3. Isobaric temperature-strain experiment under the constant tensile stress of 300 MPa along the $[111]_{B2}$ orientation. The local and bulk temperature-strain curves are reported with black and blue colors, respectively. The bulk strain was measured as 5.15%, while the local one 7.74%. DIC strain fields are reported at 300 °C, 275 °C and 150 °C during cooling. The strain fields indicate that the phase transformation is not uniform over the DIC region. In this case, the local strain measurements provide a precise estimation of the maximum transformation strain for the $[111]_{B2}$ orientation. DIC strain fields at 325 °C, 375 °C and 500 °C during heating show the reverse phase transformation.

martensite phase transformation is mostly favored. This quantity is of fundamental importance in order to provide the maximum transformation strains that can be measured for the present shape memory alloy. During the isobaric experiment, we cooled the specimen from 500 °C (fully austenitic phase) to 50 °C (fully martensitic phase). Initially, at 500 °C, the application of 300 MPa produced an initial bulk strain of 0.29%. During cooling, the phase transformation from the austenite to martensite occurs at the temperatures Ms = 316 °C and Mf = 260 °C. In the bottom of Fig. 3a the insets show the DIC strain fields during cooling. In the temperature range (300–275)°C we measured the largest strain increment. At the temperature of 300 °C, the bulk strain is 1.75% and some strain localizations are observed indicating localized martensitic regions. At 275 °C the measured bulk strain is 4.13%, while locally the strain reaches 6.68%. At the minimum temperature, 150 °C, the austenite–martensite phase transformation is complete. Using the DIC strain field at 150 °C, we identified with a blue box the sub-region where we observed the maximum local strains. The measured bulk transformation strain is 5.15%, while locally we measured 7.74%. During heating the strains are completely recovered. In the top of Fig. 3a are shown three DIC strain fields corresponding to the temperatures 325 °C, 375 °C and 500 °C (zero-stress). During heating, the transformation from the martensitic phase to the austenitic one occurs at the temperatures As = 315 °C and Af = 405 °C.

Fig. 4 shows the $[011]_{B2}$ isobaric experiment in compression. At the temperature of 330 °C, the bulk strain is 1.074% and some negligible strain localizations are measured indicating localized martensitic regions. At 305 °C the measured bulk strain is 4.13% while, locally, the strains reach 5.04%. At the minimum temperature 150 °C, the measured bulk transformation strain is 4.6%, while locally we measured 5.3%. In the bottom of Fig. 3a are shown three DIC strain fields corresponding to the temperatures 360 °C, 405 °C and 500 °C (zero-stress). Remarkably, the phase transformation is completely recoverable even at small scales as the DIC strain field at 500 °C does not show plastic strains. From this $[011]_{B2}$ isobaric experiment in compression, we measured Ms = 324 °C, Mf = 292 °C, As = 346 °C and Af = 409 °C. The transformation thermal hysteresis is the same for both the orientations and is equal to ΔT = 65 °C.

4. Discussion of the results

As reported in Figs. 3 and 4, the new $Ni_{50.3}Ti_{25}Hf_{24.7}$ shape memory alloy shows promising actuation strains associated with very high transformation temperatures (T > 400 °C). In the schematic proposed in Fig. 1, the results reported in this study are compared with the current shape memory alloys for high temperature applications. Even though NiTi are limited to temperatures below 100 °C, they show high

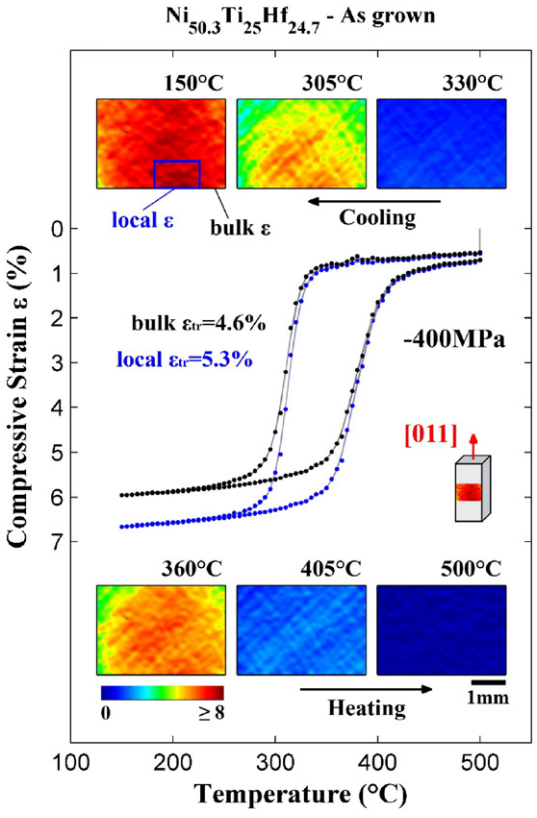

Fig. 4. Isobaric temperature-strain experiment under the constant compressive stress of 400 MPa along the $[011]_{B2}$ orientation. The bulk strain was measured as 4.6%, while the local one 5.3%. DIC strain fields are reported at 330 °C, 305 °C and 150 °C during cooling. The strain fields indicate that the crystal in the as grown condition shows a homogeneous phase transformation distribution. DIC strain fields at 360 °C, 405 °C and 500 °C during heating shows the martensite to austenite reverse transformation.

transformation strains. Remarkably, the $Ni_{50.3}Ti_{25}Hf_{24.7}$ shape memory alloy presented in this study displays comparable transformation strains along the $[111]_{B2}$ orientation. The Co–Ni–Ga transformation temperatures have improved by stress-induced martensite aging [13], and they reached the up-class NiTi + noble metal alloys. In the last years, NiTi + refractory metals have become potentially attractive shape memory alloys, in particular for cost-based reasons. Up to now, the transformation strains and temperatures of this class of shape memory alloys were limited to 4% and 200 °C, respectively. The main drawback for the industrial application of NiTiHf alloys is the limited ductility. In particular, few results in tension have shown for NiTiHf alloys with Ni > 50 at.% [5]. In this study, we demonstrated that with a precise control of the composition and the crystal orientation, NiTiHf alloys can be considered one of the best candidates for temperatures applications up to 400 °C. In fact, the tensile $[111]_{B2}$ isobaric behavior shown in Fig. 3 represents so far, one of the most promising results for high temperature applications.

The DIC strain measurements were used to detect the maximum transformation strain over small domains. Differentiating between bulk and local strains is very important as the difference between these quantities provides the degree of deformation heterogeneity of the single crystal. Moreover, the local transformation strains also indicate the maximum transformation strain obtainable along the specified crystal orientation. For the $[111]_{B2}$ tensile experiment, we obtained a bulk strain of 5.15% versus a local strain of 7.74%. In this experiment the strain field at the minimum temperature (150 °C, Fig. 3) displays a certain degree of phase transformation heterogeneity which lowers the bulk strain. Classical strain measurements technique, e. g. extensometers, cannot capture the strain heterogeneities thus lacking in recognizing the real potential of the shape memory alloy.

Even though the transformation strain for the $[111]_{B2}$ orientation in tension represents so far one of the best results achieved for NiTiHf alloys, the strain levels are still far from the ones predicted theoretically. According to our theoretical calculations based on lattice deformation theory (LDT), the phase transformation from the cubic austenitic phase to the monoclinic martensitic phase should accommodate a transformation strain of 18.93% along the $[111]_{B2}$ orientation in tension, and 9.46% along the $[011]_{B2}$ orientation in compression. Considering the local transformation strains, experimentally we obtained lower values: 7.74% for the $[111]_{B2}$ orientation in tension, and 5.3% along the $[011]_{B2}$ orientation in compression. Some observations can be obtained from the DIC strain fields reported for the $[111]_{B2}$ orientation in tension which show the largest discrepancy. In particular, it is evident from the strain fields that the transformation is heterogeneous. The DIC strain fields (strain plot at T = 150 °C in Fig. 3) suggest that this might be related to the activation of multiple martensite variants. This observation is in contrast with the assumptions of the LDT calculations where the phase transformation is supposed to occur from the single crystal austenite to the single variant martensite, thus neglecting the possibility to have multiple variants. Another source of the heterogeneous phase transformation is related to the stress level. The local DIC strain measurements for the $[111]_{B2}$ orientation in tension indicate that some plasticity arises locally. This precludes a further increment of stress, which would be necessary to complete the formation of all the possible martensite variants.

Isothermal stress–strain behaviors were also tested in a wide range of temperatures for the $[011]_{B2}$ orientation (these experiments were herein omitted for the sake of brevity). In between the temperature interval (300–400)°C, the σ_{SIM} follows the Clausius–Clapeyron equation with a slope of $(d\sigma^T/dT)_{[011]C} = 10$ MPa/°C. Moreover, for temperatures higher than T > 400 °C, slip occurs at the critical stress of 920 MPa. The critical stress to nucleate slip decreases with further temperature increment from T > 500 °C. These preliminary results indicate that this new $Ni_{50.3}Ti_{25}Hf_{24.7}$ composition holds promises also for its high level of slip resistance in the austenitic phase. This suggests that it is necessary to further investigate the orientation dependence of the NiTiHf25 alloy in order to optimize the desired transformation strains and, concurrently, the slip resistance level.

5. Conclusions

In this work we presented the high temperature actuation behavior of the new $Ni_{50.3}Ti_{25}Hf_{24.7}$ shape memory alloy. The transformation strains can reach during the isobaric experiments 7.74% in tension along the $[111]_{B2}$ orientation, and 5.3% in compression along the $[011]_{B2}$ orientation. These results paired with the high transformation temperatures measured (Af > 400 °C) suggest the new $Ni_{50.3}Ti_{25}Hf_{24.7}$ alloy as one of the most promising shape memory alloys for high temperature applications. Experimentally, we used digital image correlation in order to characterize deformation and phase transformation heterogeneity.

Acknowledgments

The work was supported by NSF-CMMI 1333884 which is gratefully acknowledged. Prof. Y. I. Chumlyakov acknowledges the support of RSF project 14-29-00012. X-ray diffraction was carried out in the Frederick Seitz Materials Research Laboratory Central Facilities, University of Illinois; the authors acknowledge Dr. Mauro Sardela for assistance with it.

References

[1] J. Ma, I. Karaman, R.D. Noebe, Int. Mater. Rev. 55 (2010) 257–315.
[2] H.E. Karaca, E. Acar, H. Tobe, S.M. Saghaian, Mater. Sci. Technol. 30 (2014) 1530–1544.
[3] S.M. Saghaian, H.E. Karaca, H. Tobe, M. Souri, R. Noebe, Y.I. Chumlyakov, Acta Mater. 87 (2015) 128–141.
[4] A.P. Stebner, G.S. Bigelow, J. Yang, D.P. Shukla, S.M. Saghaian, R. Rogers, A. Garg, H.E. Karaca, Y. Chumlyakov, K. Bhattacharya, R.D. Noebe, Acta Mater. 76 (2014) 40–53.
[5] O. Benafan, A. Garg, R.D. Noebe, G.S. Bigelow, S.A. Padula Ii, D.J. Gaydosh, N. Schell, J.H. Mabe, R. Vaidyanathan, Intermetallics 50 (2014) 94–107.
[6] H.E. Karaca, S.M. Saghaian, G. Ded, H. Tobe, B. Basaran, H.J. Maier, R.D. Noebe, Y.I. Chumlyakov, Acta Mater. 61 (2013) 7422–7431.
[7] D.R. Coughlin, P.J. Phillips, G.S. Bigelow, A. Garg, R.D. Noebe, M.J. Mills, Scr. Mater. 67 (2012) 112–115.
[8] O. Benafan, R.D. Noebe, S.A. Padula Ii, R. Vaidyanathan, Metall. Mater. Trans. A Phys. Metall. Mater. Sci. 43 (2012) 4539–4552.
[9] H.E. Karaca, S.M. Saghaian, B. Basaran, G.S. Bigelow, R.D. Noebe, Y.I. Chumlyakov, Scr. Mater. 65 (2011) 577–580.
[10] G.S. Bigelow, A. Garg, S.A. Padula Ii, D.J. Gaydosh, R.D. Noebe, Scr. Mater. 64 (2011) 725–728.
[11] L. Patriarca, H. Sehitoglu, Scr. Mater. 101 (2015) 12–15.
[12] Y. Wu, L. Patriarca, G. Li, H. Sehitoglu, Y. Soejima, T. Ito, M. Nishida, Shap. Mem. Superelast. 1 (2015) 387–397.
[13] T. Niendorf, P. Krooß, C. Somsen, G. Eggeler, Y.I. Chumlyakov, H.J. Maier, Acta Mater. 89 (2015) 298–304.